BIOCHEMISTRY
including biophysical chemistry & molecular biology

Article

pubs.acs.org/biochemistry

Reversal of the Substrate Specificity of CMP *N*-Glycosidase to dCMP

Megan D. Sikowitz,[†] Lisa E. Cooper,[‡] Tadhg P. Begley,[‡] Pierre Alexandre Kaminski,[§] and Steven E. Ealick*,[†]

[†]Department of Chemistry and Chemical Biology, Cornell University, Ithaca, New York 14853, United States

[‡]Department of Chemistry, Texas A&M University, College Station, Texas 77843, United States

[§]Institut Pasteur, Unité de Chimie et Biocatalyse, UMR CNRS 3523, 75724 Paris Cedex 15, France

Supporting Information

ABSTRACT: MilB is a CMP hydrolase involved in the early steps of biosynthesis of the antifungal compound mildiomycin. An enzyme from the bacimethrin biosynthetic pathway, BcmB, is closely related to MilB in both sequence and function. These two enzymes belong to the nucleoside 2′-deoxyribosyltransferase (NDT) superfamily. NDTs catalyze *N*-glycosidic bond cleavage of 2′-deoxynucleosides via a covalent 2-deoxyribosyl-enzyme intermediate. Conservation of key active site residues suggests that members of the NDT superfamily share a common mechanism; however, the enzymes differ in their substrate preferences. Substrates vary in the type of nucleobase, the presence or absence of a 2′-hydroxyl group, and the presence or absence of a 5′-phosphate group. We have determined the structures of MilB and BcmB and compared them to previously determined structures of NDT superfamily members. The comparisons reveal how these enzymes differentiate between ribosyl and deoxyribosyl nucleotides or nucleosides and among different nucleobases. The 1.6 Å structure of the MilB−CMP complex reveals an active site feature that is not obvious from comparisons of sequence alone. MilB and BcmB that prefer substrates containing 2′-ribosyl groups have a phenylalanine positioned in the active site, whereas NDT family members with a preference for 2′-deoxyribosyl groups have a tyrosine residue. Further studies show that the phenylalanine is critical for the specificity of MilB and BcmB toward CMP, and mutation of this phenylalanine residue to tyrosine results in a 1000-fold reversal of substrate specificity from CMP to dCMP.

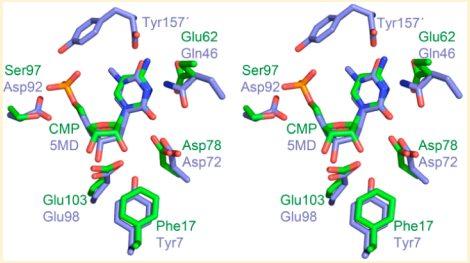

MilB is an enzyme involved in the biosynthesis of the natural product mildiomycin (Figure 1A), a commercially available antifungal agent isolated from *Streptomyces rimofaciens*.[1−3] MilB preferentially hydrolyzes the *N*-glycosidic bond of 5-hydroxymethylcytidine 5′-monophosphate (hmCMP) to release 5-hydroxymethylcytosine, which is later incorporated into mildiomycin (Figure 1B).[1] Previous studies found that MilB also hydrolyzes cytidine 5′-monophosphate (CMP) to its cytosine and ribose 5′-phosphate (Figure 1B).[1] MilB is a member of the 2′-deoxynucleoside ribosyltransferase (NDT) superfamily. Typically, NDTs catalyze the reversible transfer of 2′-deoxyribose from a donor 2′-deoxynucleoside to an acceptor base. Their structural and functional properties have been investigated in detail.[4−6] NDTs are found in a limited number of organisms and are thought to be important for nucleoside recycling when alternative nucleoside salvage pathways do not exist.[5] In contrast to most NDTs, MilB participates in a hydrolysis reaction, in which the acceptor base is replaced with a water molecule. While NDT exhibits hydrolysis activity in the absence of an acceptor base, the hydrolysis activity is ∼100-fold lower than that of its transferase reaction.[6]

BLAST analyses starting with the MilB sequence suggest homology to BcmB from *Clostridium botulinum* (47% identical sequence). Like MilB, BcmB also shows CMP hydrolase activity but is utilized in a different biosynthetic pathway. BcmB is responsible for the production of the 5-hydroxymethylcytosine precursor for the biosynthesis of bacimethrin, a thiamin antimetabolite found in *C. botulinum* (Figure 1) (T. P. Begley, manuscript in preparation). While MilB and BcmB both belong to the NDT superfamily, they differ from other members of this family in their substrate preferences. Most enzymes containing the NDT motif are specific for 2′-deoxynucleosides.[4,7] MilB and BcmB hydrolyze hmCMP, a ribonucleotide containing 5′-monophosphate and 2′-hydroxyl groups.

In addition to MilB and BcmB, several other enzymes containing the NDT motif function as nucleoside transferases. BlsM from *Streptomyces griseochromogenes* (sequence 52% identical to that of MilB) is a nucleotide hydrolase, with CMP as the preferred substrate. The cytosine produced from the BlsM reaction is incorporated into blasticidin S, a commercially available antibiotic compound (Figure 1).[8] Rcl, another member of the NDT superfamily, catalyzes the hydrolysis of purine 2′-deoxyribosyl nucleotides and is inhibited by ribonucleotides.[9] Its solution structure[10,11] and recent crystal structures with bound inhibitors[12] provide highly detailed information about its substrate−enzyme interactions. Rcl is

Received: March 11, 2013
Revised: May 6, 2013
Published: May 9, 2013

   dx.doi.org/10.1021/bi400316p | *Biochemistry* 2013, 52, 4037−4047

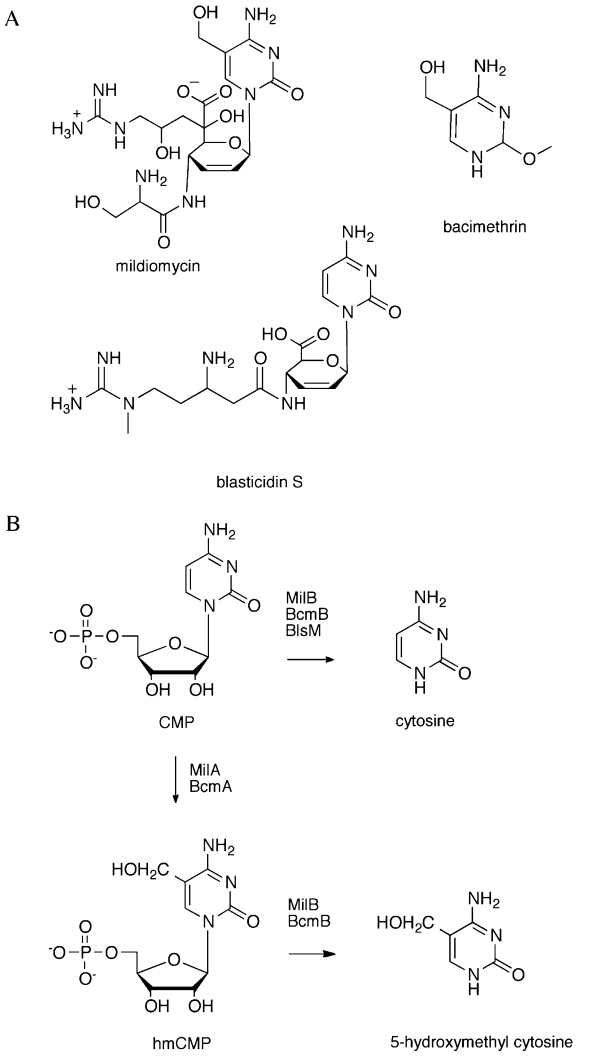

Figure 1. Natural products with cytosine precursors. (A) Cytosine, or a cytosine derivative, is incorporated in the natural products mildiomycin, bacimethrin, and blasticidin S. (B) The first steps in their biosyntheses involve the enzymatic release of cytosine or hydroxymethylcytosine from a CMP precursor by a CMP hydrolase enzyme.

unusual because it is the only NDT family member found in mammals. Rcl is upregulated in some cancers and contributes to tumorigenesis; however, the details of its cellular function are unclear.[13,14]

Because members of the NDT superfamily are not widely distributed and show significant variation in substrate specificity, their evolution is not clearly understood. Conservation of key active site residues suggests a common catalytic mechanism even though the substrates for different family members vary in their preference for ribosyl or 2′-deoxyribosyl groups, 5′-hydroxyl or 5′-phosphate groups, and the type of nucleobase. Scheme 1 shows the reaction for NDT with a

Scheme 1

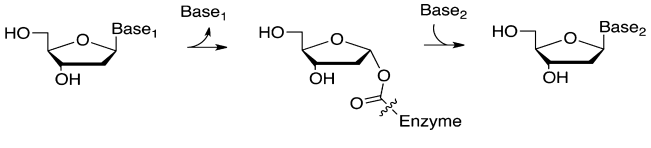

deoxyribosyl covalent intermediate, where $Base_1$ and $Base_2$ may be any purine or pyrimidine base. Each half-reaction proceeds with inversion of stereochemistry at C1′; thus, the full reaction proceeds with retention of stereochemistry.

Here we report the X-ray structures of MilB and BcmB and that of MilB complexed with CMP. Comparisons with the structures of NDT[6] and Rcl[10−12] revealed a structural basis, which was not obvious from sequence comparisons alone, by which NDT family members differentiate between ribosyl and 2′-deoxyribosyl substrates. The selectivity is attributed to a phenylalanine residue found in MilB and BcmB that is replaced with tyrosine in NDT and Rcl. In support of this hypothesis, *in vitro* enzymatic activity assays showed that for both MilB and BcmB, mutation of the active site phenylalanine residue to tyrosine resulted in a reversal of substrate preference from CMP to dCMP.

MATERIALS AND METHODS

Cloning, Expression, and Purification of MilB and BcmB. All cloning procedures followed standard DNA manipulation methods. The *S. rimofaciens* ZJU5119 *milB* gene was commercially synthesized by DNA2.0, and *bcmB* was cloned using genomic DNA from *C. botulinum* A str. ATCC 19397. The *milB* and *bcmB* genes were inserted into pTHT, a modified pET-28 plasmid (Novagen) containing an N-terminal His_6 tag and TEV protease recognition site. All mutant plasmids were prepared at the Cornell Protein Production and Purification Facility by site-directed mutagenesis of the native gene following standard, polymerase chain reaction-based mutagenesis.[15]

Escherichia coli B834(DE3), a methionine auxotrophic cell line, was transformed with the pTHT-*milB* wild-type (WT) plasmid. *E. coli* BL21(DE3) cells were used to express all other proteins. Starter cultures were grown overnight from a single colony in 10 mL of sterile LB medium containing 30 μg/mL kanamycin (LB-kan) at 37 °C while being shaken. Selenomethionine (SeMet)-containing MilB was prepared in 1.5 L cultures in minimal medium with 0.4% glucose, 1× MEM vitamin mix, 2 mM $MgSO_4$, 0.1 mM $CaCl_2$, 25 mg/L $FeSO_4$, all amino acids except methionine (20 mg/L), and 50 mg/L L-selenomethionine. To remove any LB medium during SeMet protein preparation, the overnight culture was centrifuged at 1000*g* for 20 min before the cell pellet was collected and resuspended in minimal medium. The 1.5 L volume was then inoculated with 5 mL of starter culture and allowed to grow at 37 °C while being shaken until the OD_{600} reached 0.6, at which point the incubator temperature was reduced. Once an induction temperature of 15 °C and an OD_{600} of ∼0.8 had been reached, protein expression was initiated by inoculating the cultures with 0.5 mM isopropyl β-D-thiogalactopyranoside. After 18 h, cells were centrifuged at 2000*g* for 20 min, collected, and frozen at −20 °C for storage. For native protein overexpression, 5 mL of overnight culture was added directly to 1.5 L of LB-kan medium. The cells were then grown, collected, and stored as described for the preparation of SeMet−MilB protein.

After the cell pellet had been thawed and resuspended in 45 mL of lysis buffer [50 mM Tris, 300 mM NaCl, and 20 mM imidazole (pH 8.0)], the cells were lysed on ice with two rounds of sonication. The cell extract was centrifuged for 30 min at 40000*g* and 4 °C after sonication. The supernatant was then collected and loaded onto a 2 mL Ni-NTA column (Qiagen) preequilibrated with lysis buffer. The column was

dx.doi.org/10.1021/bi400316p | *Biochemistry* 2013, 52, 4037−4047

washed with 50 mL of lysis buffer to remove any nonspecifically bound contaminants. To elute the protein, the column was washed with elution buffer [50 mM Tris, 300 mM NaCl, and 250 mM imidazole (final pH of 8.0)]. The elution sample was collected and further purified using size exclusion chromatography [HiLoad Superdex 200 PG (GE Healthcare)]. The purification procedures for WT and mutant BcmB, WT and mutant MilB, and SeMet−MilB protein all followed this protocol. The native Milb WT polyhistidine tag was removed for crystallization by incubation with TEV protease for 12 h at 4 °C. The sample was passed over a Ni-NTA column preequilibrated with lysis buffer, and the flow-through volume containing MilB was collected. The purity of the sample was analyzed by sodium dodecyl sulfate−polyacrylamide gel electrophoresis before being concentrated to ∼20 mg/mL. The protein was buffer exchanged by overnight dialysis into storage buffer [for SeMet−MilB protein, 50 mM Tris (pH 8.5) and 500 mM NaCl; for MilB WT, 10 mM Tris (pH 8.0) and 100 mM NaCl; for BcmB, 10 mM Tris (pH 8) and 50 mM NaCl] before being flash-frozen with liquid nitrogen for storage at −80 °C.

Crystallization of MilB and BcmB. The hanging-drop vapor diffusion method was used for crystallization of both MilB and BcmB. After equal volumes of the protein sample and reservoir solution had been mixed, the samples were equilibrated overnight at 18 °C against a total reservoir volume of 500 μL. Protein concentrations for crystallization were 10 mg/mL for MilB and 15 mg/mL for BcmB. Initial crystallization conditions were determined using commercially available sparse matrix screens (Hampton Research, Emerald Biosystems).

SeMet−MilB crystals grew as hexagonal rods approximately 200 μm long and 40 μm wide under the optimized crystallization condition of 8% PEG 1000, 0.1 M phosphate-citrate (pH 4.2), and 0.2 M Li_2SO_4 after 2 days. A second condition for MilB crystallization was found with the N-terminal polyhistidine tag removed. Square rods 400 μm long and 20 μm wide crystallized after 2 days in 0.1 M Tris (pH 7.5), 0.2 M $MgCl_2$, and 18% PEG 8000. The ligand was soaked into the crystals using a solution containing the components of the reservoir solution supplemented with 10 mM cytosine and 10 mM ribose 5-phosphate for 5 min before cryoprotection.

BcmB crystals formed 200 μm × 150 μm plates with a thickness of 10 μm in 18% PEG MME 2000, 0.1 M phosphate-citrate (pH 4.4), 0.01 M spermine, and 0.2 M $(NH_4)_2SO_4$ after 5 days. All crystals were cryoprotected with a solution consisting of their crystallization condition supplemented with 20% ethylene glycol before being flash-frozen with liquid nitrogen.

Data Collection and Processing. X-ray diffraction experiments were conducted on Advanced Photon Source NE-CAT beamline 24-ID-C (Argonne National Laboratory, Argonne, IL) using a Quantum315 detector (Area Detector Systems Corp.) using vitrified crystals. A fluorescence scan was conducted to determine the data collection wavelength corresponding to the maximal f'' for the SeMet−MilB crystals. All data collection runs used the oscillation method with 1.0° of rotation per frame. HKL2000 was used for indexing, integrating, and scaling the data.[16] Data collection and processing statistics are listed in Table 1.

Structure Determination, Model Building, and Refinement. The crystal structure of MilB was determined by single-wavelength anomalous diffraction (SAD) using SeMet−MilB protein. The crystals belong to space group $P6_222$ with a Matthews coefficient of 2.1 Å^3/Da and an estimated solvent content of 41%, assuming one protein chain per asymmetric unit.[17] Initial-phase calculation and model building were conducted using PHENIX AutoSol.[18,19] Subsequent model improvement was performed using COOT[20] for manual manipulations and PHENIX.refine[19] with default parameters for structure refinement. Water molecules were added during later rounds of refinement in PHENIX, and the final structure was analyzed using COOT and MolProbity.[21] The structure of MilB complexed with CMP was determined in space group $C2$ with two protein chains per asymmetric unit. Under this new

Table 1. Summary of Data Collection and Refinement Statistics[a]

	SeMet−MilB−SO_4	MilB−CMP	BcmB−PO_4
beamline	APS 24-ID-C	APS 24-ID-C	APS 24-ID-C
resolution (Å)	1.95	1.55	2.99
wavelength (Å)	0.97918	0.97918	0.97918
space group	$P6_222$	$C2$	$C2$
a (Å)	97.8	45.2	177.9
b (Å)	97.8	100.4	40.2
c (Å)	61.9	71.5	98
β (deg)	90.0	99.6	98.0
Matthews coefficient	2.1	2.1	3.2
% solvent	41	41	61
no. of molecules per asymmetric unit	1	2	3
no. of measured reflections	137124	162974	54150
no. of unique reflections	23697	44996	14604
average I/σ	37.1 (5.3)	25.1(3.6)	17.8 (4.7)
redundancy	5.7 (5.4)	3.6(3.6)	3.7(3.8)
completeness (%)	98 (97)	99.8 (100)	99.9(100)
R_{sym} (%)[b]	5.4 (32.1)	5.7 (35.2)	10.0(34.2)
no. of protein atoms	1164	2369	2700
no. of ligand atoms	10	41	15
no. of water atoms	96	196	10
no. of reflections in the working set	23686	42663	14582
no. of reflections in the test set	1168	2269	737
R factor/R_{free} (%)[c]	20.6/25.2	19.9/22.7	20.7/23.9
rmsd from ideals			
bonds (Å)	0.007	0.006	0.015
angles (deg)	1.072	1.061	1.975
average B factor for protein (Å^2)	28.1	18.0	49.1
average B factor for water (Å^2)	34.1	25.6	54.5
average B factor for ligand (Å^2)	31.3	17.0	84.2
Ramachandram plot (%)			
most favored	97.3	98.0	96.3
allowed	2.7	2.0	3.7
disallowed	0.0	0.0	0.0

[a]Values in parentheses are for the highest-resolution shell. [b]$R_{sym} = \sum\sum_i|I_i - \langle I\rangle|/\Sigma\langle I\rangle$, where $\langle I\rangle$ is the mean intensity of N reflections with intensities I_i and common indices h,k,l. [c]$R_{work} = \sum_{hkl}||F_{obs}| - k|F_{cal}||/\sum_{hkl}|F_{obs}|$, where F_{obs} and F_{cal} are observed and calculated structure factors, respectively, calculated over all reflections used in the refinement. R_{free} is similar to R_{work} but calculated over a subset of reflections (5%) excluded from all stages of refinement.

dx.doi.org/10.1021/bi400316p | Biochemistry 2013, 52, 4037−4047

condition, MilB also crystallized with a Matthews coefficient of 2.1 Å^3/Da corresponding to a 41% solvent content. SKETCHER was used for ligand generation before placement into $F_{obs} - F_{cal}$ electron density.[22] Model improvement was performed as described above.

BcmB crystallized in space group C2 with three chains per asymmetric unit and a Matthews coefficient of 3.2 Å^3/Da, corresponding to a solvent content of approximately 61%. The structure of BcmB was determined using molecular replacement, with the newly determined MilB structure as the search model.[23] MolRep placed three chains in the asymmetric unit, and further model building and refinement were conducted using COOT and Refmac.[20,24] The three chains correspond to one dimer formed through noncrystallographic 2-fold symmetry and one dimer generated by crystallographic symmetry. Several rounds of refinement using Refmac and PHENIX.refine resulted in a BcmB model with R factor and R_{free} values of 21.7 and 24.2%, respectively. Refinement statistics for SeMet−MilB, MilB−CMP, and BcmB are summarized in Table 1.

Analytical High-Performance Liquid Chromatography (HPLC). Reaction mixtures were analyzed by reverse-phase HPLC on an Agilent 1200 HPLC system equipped with a quaternary pump and thermostated autosampler (4 °C). The stationary phase was a Supelcosil LC-18-T column (15 cm × 4.6 mm, 3 μm particles). The LC eluent (flow rate of 1 mL/min) consisted of a gradient of methanol and 6 mM *N*,*N*-dimethylhexylamine (DMHA) in water that was adjusted to pH 6.5 by addition of acetic acid. In the analytical method, the percentages of DMHA (D) and methanol (M) balanced with water at time t varied according to the following scheme: (t,M,D), (0,0,100), (2,10,80), (12,20,60), (14,65,10), (16,0,100), (21,0,100). Chromatograms were detected using the absorbance at 270 nm. UV−vis spectra of substrate and product peaks were also collected and assessed.

Substrate Specificity for MilB and BcmB. Substrate specificity studies of MilB and MilB F17Y were conducted with adenosine 5′-monophosphate (AMP), CMP, 2′-deoxycytidine 5′-monophosphate (dCMP), guanosine 5′-monophosphate (GMP), and inosine 5′-monophosphate (IMP) (Figure S1 of the Supporting Information). Experiments were designed on the basis of the previously described assay conditions used for MilA and MilB.[25] *In vitro* enzymatic assays were prepared with a final volume of 50 μL. AMP, CMP, dCMP, GMP, or IMP (1 mM) was added to MilB WT or MilB F17Y (10 μM) in 50 mM Tris buffer (pH 7.5), and then the samples were incubated at 37 °C for 3 h. Control samples without enzyme were also prepared. Reactions were quenched by boiling mixtures at 100 °C for 5 min. Samples were diluted with DMHA, filtered using a 3 kDa molecular mass cutoff membrane, and analyzed by HPLC as described above. Reaction products were compared to commercially available standards that were analyzed under identical conditions. Substrate specificity studies for BcmB and BcmB F6Y were conducted with CMP and dCMP as described above.

Kinetics of MilB and BcmB. Kinetic parameters were monitored on the basis of production of cytosine from CMP or dCMP for MilB WT, MilB F17Y, BcmB WT, and BcmB F6Y. Each enzyme was incubated with varying substrate concentrations (see Table S1 of the Supporting Information) in 50 mM Tris (pH 7.5) for 30 min at 37 °C, and then the reactions were quenched by boiling the mixtures at 100 °C for 5 min. Samples were diluted with DMHA, filtered using a 3 kDa molecular mass cutoff membrane, and analyzed by HPLC as described above. Reaction products were compared to commercially available standards that were analyzed under identical conditions. The product absorbance signal was measured by integration (ChemStation, Agilent Technologies) and compared to cytosine standards at known concentrations. Kinetic parameters were calculated using the Michaelis−Menten function in KaleidaGraph version 4.0 (Synergy Software).

Figure Preparation. All figures were prepared using PyMOL,[26] ChemDraw (Cambridge Biosoft), KaleidaGraph version 4.0 (Synergy Software), or Excel (Microsoft) and compiled in Photoshop (Adobe).

RESULTS

Structure of MilB. The MilB with bound SO_4 contains one protomer per asymmetric unit; however, a dimer is formed by crystallographic 2-fold symmetry. The final model at 1.95 Å resolution contains residues 11−162 of the 170 possible amino acid residues. The protomer of MilB contains an α/β-fold with a five-stranded parallel β-sheet with a strand order of 21345 (flavodoxin-like). The β-sheet is flanked on both sides by α-helices in an asymmetric manner (Figure 2A,B). Dimer

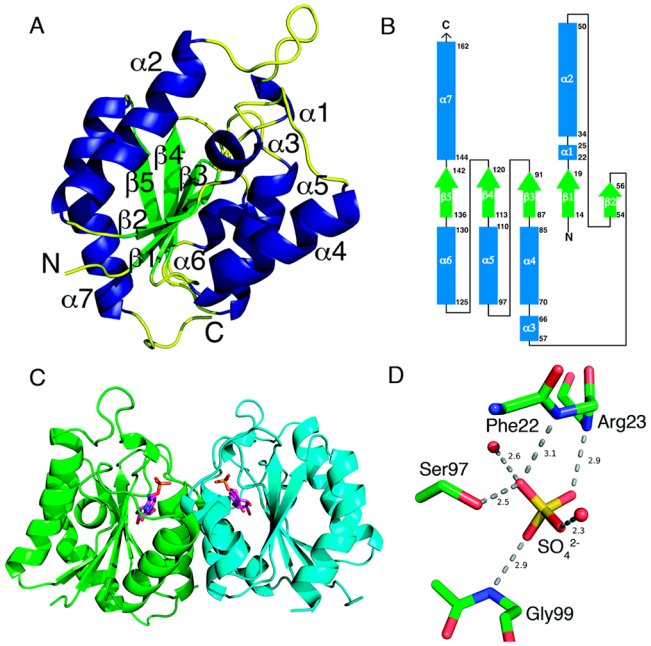

Figure 2. Structure of MilB. (A) The MilB protomer structure adopts an overall α/β-twist fold, depicted with green β-strands and blue α-helices. (B) Topology diagram of MilB with light green β-strands and light blue α-helices. (C) Dimeric structure of MilB with chain A colored green and chain B cyan and ligands bound in the active sites. (D) Active site phosphate-binding pocket occupied by a sulfate ion in the MilB−SO_4 complex. The sulfate binding site corresponds to the phosphate binding site in the CMP complex.

formation occurs through interactions among helices α4−α6 of the two protomers with an interface area of 1170 Å^2. Size exclusion chromatography confirmed the dimeric state of MilB (data not shown), which is consistent with the quaternary structures of both NDT (trimer of dimers) and Rcl.

The MilB−CMP complex also crystallizes with one dimer per asymmetric unit. The final model at 1.55 Å resolution contains residues 12−168 of chain A and residues 10−162 of chain B. Each protomer is occupied by one CMP molecule, and

dx.doi.org/10.1021/bi400316p | *Biochemistry* 2013, 52, 4037−4047

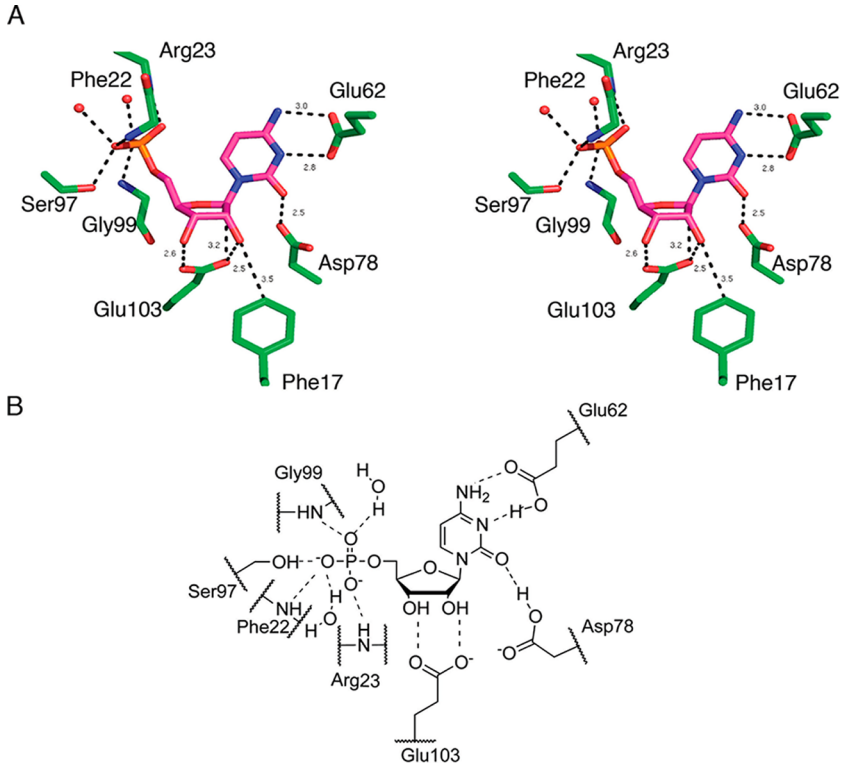

Figure 3. Substrate binding in MilB. (A) MilB−CMP binding interactions represented as sticks. (B) Schematic diagram of the MilB active site with CMP bound.

the overall structure is essentially the same as that of the MilB−SO_4 complex. Each dimer features two equivalent active sites.

MilB Active Site. The MilB active site is located at the C-terminal edge of the β-sheet, between helices α4 and α5 (Figure 2C). All of the interactions necessary for substrate binding and catalysis occur within a single MilB protomer, with no direct participation from the adjacent protomer. A phosphate/sulfate binding pocket contains hydrogen bonding interactions with the Ser97 side chain, the amide groups of Gly99, Arg23, and Phe22, and two well-ordered water molecules (Figure 2D). This binding site corresponds to the phosphate binding site in the CMP complex. Ordered water molecules occupy the rest of the active site in the MilB−SO_4 structure.

The structure of the MilB−CMP complex provides the molecular details of the nucleobase and ribosyl binding sites (Figure 3). The products of the CMP hydrolysis reaction, cytosine and ribose 5-phosphate, were soaked into the MilB crystals. Continuous electron density is observed in the active site representing CMP, the product of the reverse reaction, yet our *in vitro* studies did not show significant formation of CMP upon incubation of MilB, cytosine, and ribose 5-phosphate (data not shown). Thus, the presence of CMP in the active site of the MilB−CMP complex is a result of enzyme activity despite the fact that we could not detect activity *in vitro*. Glu62 accepts a hydrogen bond from the 4-amino group of the cytosine base and, if protonated, would donate a hydrogen bond to N5 of CMP. Glu103 accepts hydrogen bonds from the 2′- and 3′-hydroxyl groups of CMP. Additionally, the side chain of Asp78 is within hydrogen bonding distance of O2 of the cytosine. C4 of Phe17 is 3.5 Å from the 2′-oxygen of CMP in the MilB structure.

Structure of BcmB. BcmB crystallized in space group *C*2, with three protein chains in the asymmetric unit. The structure of BcmB was determined to 3.0 Å resolution using the MilB structure (47% identical sequence) described above as the molecular replacement search model. The protomeric structure of BcmB displays the same α/β-twist fold as MilB, with five parallel β-strands forming a parallel β-sheet flanked on either side by α-helices (Figure S2A,B of the Supporting Information). The final BcmB model contains 120 amino acids in chain A, 123 in chain B, and 110 in chain C. The missing regions include residues 11−20 and 110−113 in chain A, 11−21 and 112 in chain B, and 10−24 and 109−112, which correspond to loop regions. Missing residues 47−55, 48−56, and 46−58 in protomers A−C, respectively, correspond to a short α-helix and loop when aligned with MilB.

Chains A and B form a dimer by 2-fold noncrystallographic symmetry. The buried surface area at the interface is 1320 Å^2. Chain C forms a dimer with an equivalent chain C using crystallographic 2-fold symmetry. The buried surface area of this interaction is 1210 Å^2. This small discrepancy between the A−B and C−C interface surfaces areas can be attributed to additional disordered regions in chain C. Residues 58 and 59 in chains A and B and residue 114 in chain A are present at the A−B dimer interface but are disordered at the C−C dimer interface. The oligomeric state of BcmB observed in the crystal structure is supported by size exclusion chromatography results (data not shown) and closely resembles the dimer formed by MilB (Figure S2C of the Supporting Information).

BcmB Active Site. The active site of BcmB is similar to that of MilB. Each active site contains a bound phosphate ion from the crystallization solution. The phosphate makes hydrogen bonds with the side chain of Ser86 and the amide backbone of Gly88 in the phosphate-binding pocket (Figure S2D of the

dx.doi.org/10.1021/bi400316p | *Biochemistry* 2013, 52, 4037−4047

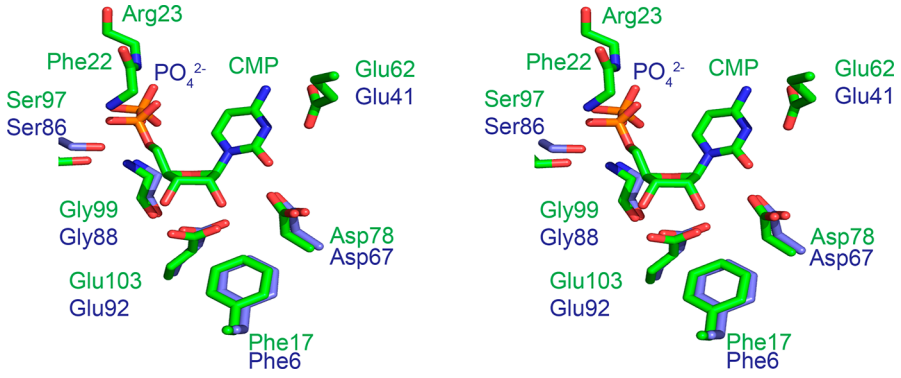

Figure 4. BcmB−PO_4 and MilB−CMP complex active site comparison. Stereoview of BcmB−PO_4 and MilB−CMP complex active sites superimposed. The active site residues of BcmB (blue) and MilB (green) display a conserved architecture. Glu41 is disordered in the BcmB structure but conserved in sequence with Glu62 of MilB.

Supporting Information). On the basis of structural comparison to MilB, the BcmB active site residues that participate in substrate binding include Asp67, Glu92, and Phe6 (Figure 4). Glu41 falls in a disordered region in the BcmB crystal structure but is expected to be equivalent to Glu62 in MilB on the basis of sequence alignments.

Kinetics and Substrate Specificity of MilB and BcmB. Initial studies determined the substrate specificity of MilB for cytosine-containing nucleotides.[1] MilB preferentially hydrolyzed CMP, but cytosine formation was also observed, to a lesser extent, with dCMP (Figure 5). MilB showed little to no hydrolysis of purine-containing substrates (Figure S1 of the Supporting Information). CMP or dCMP was incubated with MilB F17Y, and the production of cytosine was monitored to measure *N*-glycosidase activity. MilB F17Y successfully cleaved dCMP but was no longer able to effectively hydrolyze CMP (Figure 5). Similar studies were conducted for both BcmB WT and the corresponding active site Phe mutant (F6Y). As with MilB WT, BcmB WT can hydrolyze CMP and, to a lesser extent, dCMP (Table 2). Conversely, BcmB F6Y hydrolyzed dCMP with a 2′-deoxyribosyl group, while showing only minor activity with CMP (Figure S3 of the Supporting Information).

Steady-state kinetic parameters were determined for MilB WT, MilB F17Y, BcmB WT, and BcmB F6Y using either CMP or dCMP as the substrate (Table 2). The k_{cat}/K_M value for MilB WT with hmCMP was previously reported to be 22.1 M^{-1} s^{-1}.[1] The k_{cat}/K_M values observed for hydrolysis of CMP and dCMP by MilB WT were 5.2 and 1.1 M^{-1} s^{-1}, respectively.[1]

DISCUSSION

Structural Comparison. MilB and BcmB both adopt an α/β-fold composed of five parallel β-strands forming a core β-sheet flanked on either side by several α-helices. This fold is highly conserved among the NDT superfamily enzymes. A pairwise DALI comparison between the MilB and BcmB structures results in a *Z* score of 16.9 and an rmsd of 1.7, confirming their highly conserved tertiary structure (Table 3).[27] A DALI structure search against the Protein Data Bank (PDB) starting with MilB reveals structural homology to the known 2′-deoxyribosyltransferases and Rcl (Table 3). Though their levels of sequence identity are relatively low (11−22%), the enzymes retain similar folds. On the basis of a *Z* score of 15.5 with an rmsd of 2.3 Å, MilB is the most structurally similar to *Rattus norvegicus* Rcl (PDB entry 4FYI).[12] Similar rmsds of 2.5 and 2.9 Å are observed upon comparison of MilB to the Rcl solution

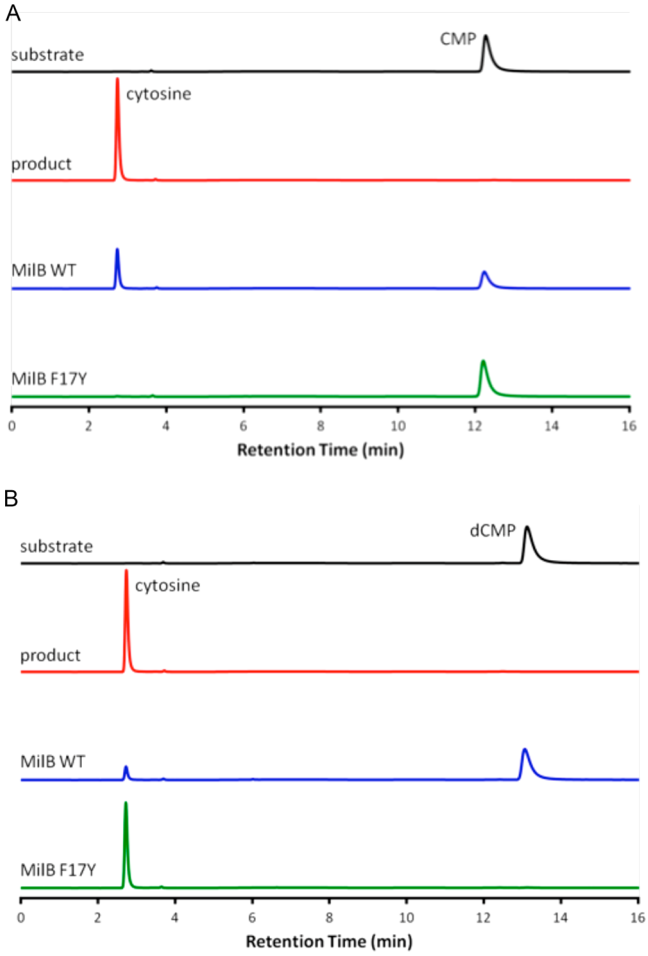

Figure 5. Substrate specificity of MilB WT and MilB F17Y. (A) When MilB WT is incubated with CMP, a large peak representing free cytosine is observed. For MilB F17Y incubated with CMP, little hydrolysis is observed. (B) The opposite effect is observed with dCMP as the substrate. MilB F17Y hydrolyzes dCMP, producing free cytosine. There is comparably less dCMP hydrolysis by MilB WT.

structures with PDB entries 2KHZ[11] and 2KLH,[10,11] respectively. Several 2′-deoxyribosyltransferases, such as the *Trypanosoma brucei*[30] and *Lactobacillus leichmannii*[6,28,29] NDTs (PDB entries 2F2T and 1F8X) and *Lactobacillus helveticus* purine nucleoside 2′-deoxyribosyltransferase (PTD) (PDB entry 1S2L),[29] are also among the most homologous structures.

dx.doi.org/10.1021/bi400316p | *Biochemistry* 2013, 52, 4037−4047

Table 2. Summary of Kinetic Data

protein (substrate)	k_{cat} (min^{-1})	K_M (mM)	k_{cat}/K_M (M^{-1} s^{-1})
MilB WT (CMP)	1.19 (0.06)	3.8 (0.5)	5.2 (0.7)
MilB WT (dCMP)	0.36 (0.02)	5.4 (0.8)	1.1 (0.2)
MilB F17Y (CMP)	0.0126 (0.0003)	4.5 (0.4)	0.046 (0.004)
MilB F17Y (dCMP)	7.6 (0.3)	1.2 (0.2)	100 (10)
BcmB WT (CMP)	0.090 (0.003)	0.19 (0.02)	7.8 (0.9)
BcmB WT (dCMP)	0.055 (0.001)	0.57 (0.05)	1.6 (0.1)
BcmB F6Y (CMP)	0.0048 (0.0004)	0.9 (0.2)	0.09 (0.02)
BcmB F6Y (dCMP)	0.081 (0.001)	0.042 (0.004)	32 (3)

Table 3. Enzymes Structurally Similar to MilB

protein	PDB entry	Z score	rmsd	% identity	no. of aligned residues
C. botulinum BcmB	4JEL	16.9	1.7	46	123
R. norvegicus Rcl	4FYI	15.5	2.3	21	126
R. norvegicus Rcl (NMR)	2KHZ	14	2.5	22	134
R. norvegicus Rcl (NMR)	2KLH	13.7	2.9	21	131
T. brucei NDT	2F2T	12	2.8	13	126
L. helveticus PTD	1S2L	11.9	2.4	19	122
L. leichmannii NDT	1F8X	10.6	2.8	11	123

While the enzymes in the NDT superfamily maintain a similar tertiary structure, their oligomeric assembly is not fully conserved. Both NDTs and PTD form a hexamer composed of a trimer of homodimers, while Rcl, MilB, and BcmB are observed to form only dimers.[6,11,28] Comparison of the dimer interfaces reveals a conserved mode of interaction (Figure 6). Like those of many members of the NDT superfamily,[10] the interactions observed at the dimer interfaces in MilB and BcmB are mainly hydrophobic (>97%).

Base Specificity. Structural analysis of MilB, BcmB, and related enzymes reveals the basis of their substrate specificities.

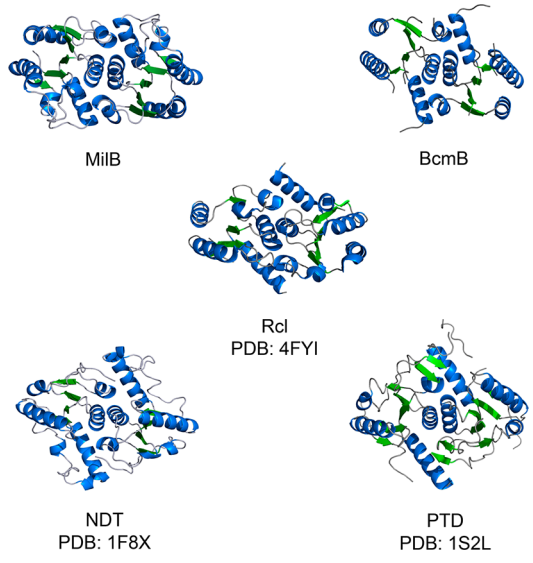

Figure 6. Comparison of enzyme dimerization. MilB and BcmB are observed to be dimers. Like MilB, BcmB and Rcl have a dimeric tertiary structure. In their functional forms, NDT and PTD are hexamers composed of a trimer of dimers, in which the dimer (shown) is similar to that of MilB.

MilB shows specificity for the pyrimidine-containing hmCMP or CMP substrates. It does not hydrolyze the purine-containing nucleotides, demonstrated by an inability to hydrolyze AMP, GMP, or IMP (Figure S1 of the Supporting Information). While highly specific for hmCMP or CMP, its relatives display variable nucleobase specificity (Table 4). NDT accepts all naturally occurring and some synthetic nucleosides, while PTD[30] and Rcl[7] are specific for purine-containing nucleosides and nucleotides, respectively. In the structure of the MilB–CMP complex, the Glu62 carboxylic group is ~3 Å from the cytosine, forming hydrogen bonds with the cytosine N3 and 4-amine group (Figure 3). Helix α3 (on which Glu62 is located), helix α4, and the loop region formed by residues 67–70 shield the MilB active site. As a result, MilB has a relatively compact substrate binding site that cannot accommodate the bulkier purine-containing nucleotides. The specificity of BcmB is predicted to function like that of MilB based on sequence and structural homology.

The carboxylic acid from the NDT C-terminal Tyr157′ and the Gln46 amine interact with its substrate nucleobase. NDT can accommodate a variety of nucleobases because of its flexibility in both accepting and donating hydrogen bonds.[6] Like NDT, PTD interacts with nucleobases via hydrogen bonds from the carboxylic tail of the C-terminal tyrosine located in the active site. PTD diverges from NDT, as there are no interactions equivalent to those provided by Gln46 in NDT.[28] The complexed Rcl structures[10−12] reveal a large nucleobase binding area with no specific enzyme–nucleobase interactions, allowing Rcl to accommodate a variety of nucleobases in its active site. Because the Rcl active site is rather open, it is solvent accessible and favors the larger purine-containing substrates that can aid in shielding the active site from the solvent. As evidenced by the structures of MilB and other NDT superfamily members, their nucleobase specificities are derived from a combination of favorable enzyme–substrate hydrogen bonding interactions and active site accessibility.

Specificity at the 5′-Position. The NDT family members differ in their substrate preference for either a hydroxyl or phosphate group at the 5′-position (Table 4). The high-resolution MilB–CMP structure reveals key information about the enzyme–substrate binding interactions at the CMP 5′-position, including seven hydrogen bonds. Two ordered water molecules each contribute one hydrogen bond, while Ser97 is within hydrogen bonding distance of either of the two 5′-phosphate oxygen atoms. While the active site serine residue observed in MilB is conserved in both BcmB and BlsM (Figure 7), the remaining interactions in the MilB phosphate binding pocket come from amide backbone groups and ordered water molecules. The amide backbones of Phe22, Arg23, and Gly99 act as hydrogen bond donors, completing the phosphate binding pocket (Figure 8A). Although the identities of the backbone residues are not conserved in sequence, the phosphate ion in the BcmB–PO_4 complex is observed in a binding pocket analogous to that of MilB (Figure 8B). This pocket is also rich with hydrogen bond donors, resulting in a preference for phosphate groups at the 5′-position.

A 5′-phosphate binding pocket utilized for nucleotide binding was also observed in Rcl.[10−12] The structure of Rcl shows hydrogen bonding contacts between the GMP phosphate group and Ser17, Arg19, Ser87, and Ser117′ (Figure 8B). This motif is highly conserved in the sequences of 13 different species in Rcl.[10] While MilB does not share this motif, the positively charged pocket is consistent with a preference for

dx.doi.org/10.1021/bi400316p | *Biochemistry* 2013, 52, 4037–4047

Table 4. Summary of NDT Superfamily Enzymes

enzyme	preferred base	5′-specificity	2′-specificity	acceptor/nucleophile
MilB	hydroxymethylcytosine/cytosine	phosphate	OH	water
BcmB	hydroxymethylcytosine/cytosine	phosphate	OH	water
BlsM	cytosine	phosphate	OH	water
Rcl	purine	phosphate	H	water
NDT	purine/pyrimidine	OH	H	purine/pyrimidine
PTD	purine	OH	H	purine

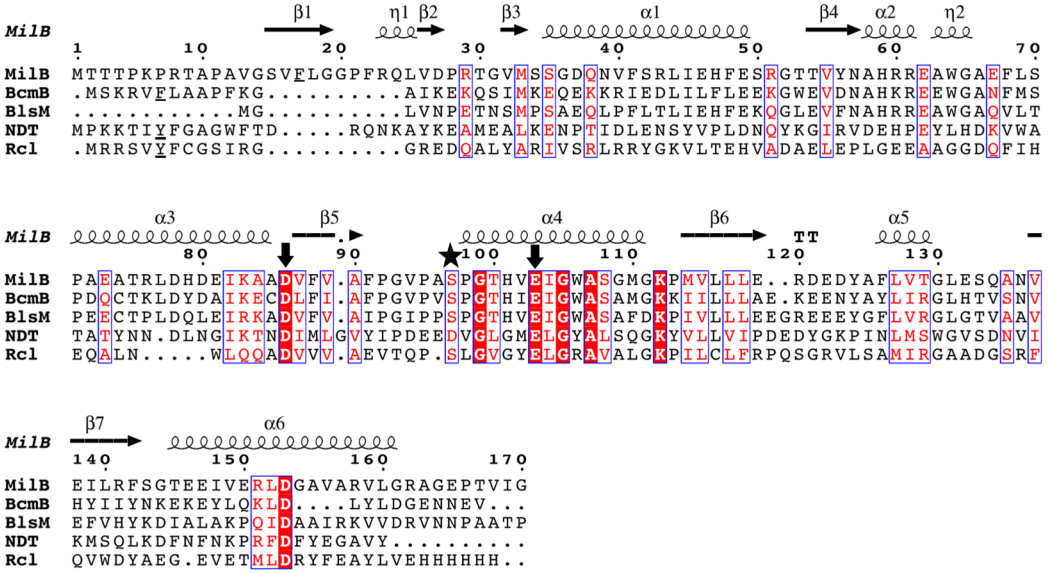

Figure 7. Sequence alignment of enzymes containing the nucleoside 2′-deoxyribosyltransferase motif. Sequence comparison between the MilB–BcmB complex and other family members reveals conservation of the key catalytic residues (arrows) but not those conferring substrate binding specificity. The serine residue involved in phosphate binding is denoted with a star. Phenylalanine and tyrosine residues known to be positioned in the active site are underlined. Representative sequences for NDT from *L. leichmannii* and Rcl from *R. norvegicus* were used.

nucleotide monophosphate binding. In NDTs and PTD, an aspartate residue and either an asparagine or glutamine residue stabilize nucleoside 5′-hydroxyl groups, favoring nucleoside binding (Figure 8C)[6,28] and preventing the binding of 5′-phosphate-containing nucleotides preferred by MilB and BcmB.[4]

Specificity at the 2′-Position. While MilB and BcmB contain the conserved NDT motif, their ability to hydrolyze the *N*-glycosidic bonds of ribosylnucleotides makes them unique from other enzymes in this class. NDTs, PTD, and Rcl show no glycosidase activity toward ribosyl-containing substrates, which in some cases are inhibitory.[9] Conversely, MilB and BcmB show higher activity toward substrates containing 2′-hydroxy groups (Table 2). In the related Rcl and NDT structures, a tyrosine residue is observed near the substrate 2′-binding position (Figure 8). Not obvious from sequence analysis alone, the structures of MilB and BcmB reveal a phenylalanine in the position equivalent to this tyrosine near the conserved catalytic glutamate (Figure 7). Compared to that of Rcl or NDTs, this phenylalanine residue is the only residue near the 2′-binding position that differs in either MilB or BcmB.

The identity of the active site phenylalanine or tyrosine residue proves to be important in differentiating between ribosyl- or deoxyribosyl-containing substrates by MilB and BcmB. Structural studies of PTD,[28] which has a tyrosine residue near the 2′-binding position, suggested that ribosylated substrates form hydrogen bonds with the catalytic glutamate, rendering it unreactive. This rational contradicts our findings in which MilB and BcmB react with ribosylated substrates, despite also showing interactions between their catalytic glutamate and the substrate 2′-hydroxyl group. When both a 2′-hydroxyl-containing substrate and active site tyrosine are present, the glutamate may be too constricted by hydrogen bonds to position itself for catalysis. In the absence of an active site tyrosine, the catalytic glutamate is not restricted by the ribosylated substrate. Rather, the ribosylated substrate may help orient the glutamate for catalysis.

Acceptor/Nucleophile Binding Site. Previous studies of NDT superfamily members have explored the structural basis of nucleophile binding at the active site. In NDT, the interaction between Gln46 and the nucleobase positions the loop region, on which Gln46 is located, shielding the active site from solvent.[28] Along with a hydrophobic binding pocket, this excludes water as a nucleophile. After initial *N*-glycosidic bond cleavage and release of the base, NDT binds the incoming acceptor base, positioning it for the second half of the NDT transferase reaction. Because of more limited substrate–enzyme interactions in PTD, the corresponding loop region does not shield its active site[28] and bulkier purine bases that shield the active site are favored over smaller pyrimidines, as both substrate and acceptor nucleobases. Compared to NDT, Rcl has a longer loop region that does not shield the active site from solvent. It also does not have any residues that specifically interact with and bind acceptor nucleobases.[10−12] These structural features allow a water molecule to act as the final acceptor. Because the MilB active site is shielded by α-helices, it

dx.doi.org/10.1021/bi400316p | *Biochemistry* 2013, 52, 4037−4047

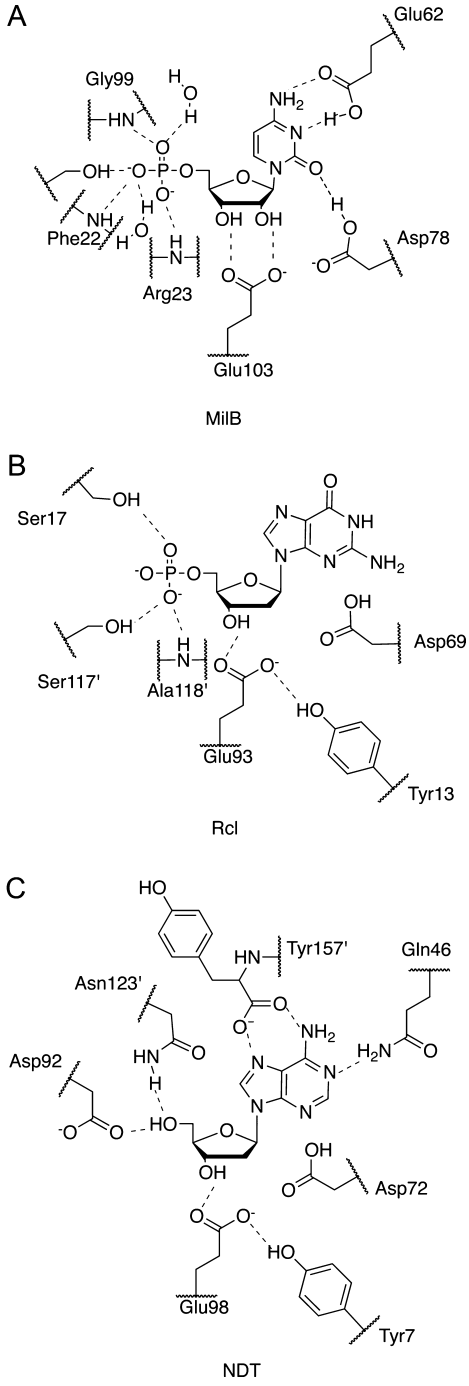

Figure 8. Active site comparison. (A) Observed interactions of MilB with CMP. (B) Rcl active site with dGMP. (C) NDT active site with deoxyadenosine.

is less solvent accessible than that of PTD or Rcl. Compared to that of NDT, the MilB active site is similarly shielded but is not as hydrophobic. As a result, an active site water molecule is available to act as the final acceptor. Accordingly, the MilB–CMP structure reveals a water molecule in the active site positioned 4.9 Å from the 1′-ribosyl position.

Mechanism of Hydrolysis. Previous studies showed that NDT family members catalyze transferase reactions utilizing a covalent enzyme-(deoxy)ribosyl intermediate.[6,9,31] In the first half-reaction, the covalent intermediate forms between a glutamate side chain and C1′ of the (deoxy)ribosyl group (Scheme 1). The second half-reaction takes place after the purine/pyrimidine base is released and a nucleophile (either a different base or a water molecule) displaces the glutamate side chain. Each half-reaction is inverting at C1′ such that the stereochemistry at C1′ is retained for the full reaction. The catalytic glutamate residue is absolutely conserved among the NDTs, Rcl, MilB, BcmB, and BlsM (Figure 8). On the basis of this mechanism, Glu103 of MilB forms a covalent attachment to CMP at the ribosyl C1′ position in the first half of the hydrolysis reaction (Scheme 2). Previous studies on xylanases, which utilize a glutamate/glycoside covalent intermediate in a hydrolysis reaction similar to that of MilB, showed that each half-reaction proceeds through an oxocarbenium-like transition state.[32] In the crystal structure of the MilB–CMP complex, the glutamate oxygen atom is not correctly oriented for a strictly S_N2 mechanism, suggesting the formation of an oxocarbenium ion intermediate followed by trapping of the intermediate by Glu103. The second half-reaction, in which water displaces the glutamate side chain, likely proceeds through an oxocarbenium-like transition state. In MilB, Asp78 is positioned to protonate the cytosine base leaving group and to activate a water molecule for the second half of the reaction. This aspartate residue is conserved in MilB, BcmB, BlsM, and Rcl, also suggesting a conserved mechanism of hydrolysis.

Reversal of Substrate Specificity. On the basis of the structural data, we hypothesized that the active site phenylalanine is the key residue that confers specificity for either 2′-hydroxyl or 2′-deoxy groups. In MilB, C4 of Phe17 is 3.6 Å from the catalytic glutamate residue and 3.5 Å from the CMP 2′-hydroxyl group. A tyrosine is at a position equivalent to Phe17 of MilB in all previously determined structures of enzymes in the NDT superfamily, which prefer 2′-deoxy substrates (Figure 9). MilB F17Y was constructed using site-directed mutagenesis and used to test if the phenylalanine to tyrosine change is sufficient to increase the efficiency of dCMP hydrolysis. While MilB WT preferentially hydrolyzes CMP, with a 5-fold lower efficiency toward dCMP, the F17Y mutation of MilB resulted in a 100-fold decrease in the level of hydrolysis of CMP and a 100-fold increase in the level of hydrolysis of dCMP, corresponding to a >10000-fold inversion of substrate specificity (Table 2). A similar but slightly smaller effect on substrate specificity was observed for BcmB.

The largest change is seen in the preference of MilB F17Y for dCMP over CMP. The k_{cat} value of MilB WT with CMP is ~3-fold larger than that with dCMP. For MilB F17Y, the value of k_{cat} with dCMP is ~600-fold larger than with CMP. For both MilB WT and F17Y, the K_M values for both substrates are in a similar range, with the value for MilB F17Y with dCMP being the lowest. The k_{cat} value of BcmB WT with CMP is ~20-fold larger than that with dCMP. For BcmB F6Y, the k_{cat} with dCMP is ~20-fold larger than that with CMP. The K_M values for WT and mutant BcmB show a larger range than those of MilB. The lowest value is 0.042 mM for BcmB F6Y with dCMP, and the highest value is 0.9 mM for BcmB WT with dCMP.

In the MilB–CMP structure, the CMP 2′-hydroxyl group interacts with the catalytic Glu103, orienting the molecule in the active site. On the basis of the location of the Phe17 in the MilB–CMP structure, the MilB F17Y Tyr17 hydroxyl group would be 3.1 Å from the 2′-hydroxyl group of bound CMP. This may cause unfavorable interactions for CMP binding or electronic repulsions effecting hydrolysis by the catalytic glutamate residue. The latter is consistent with the observed

dx.doi.org/10.1021/bi400316p | *Biochemistry* 2013, 52, 4037–4047

Scheme 2

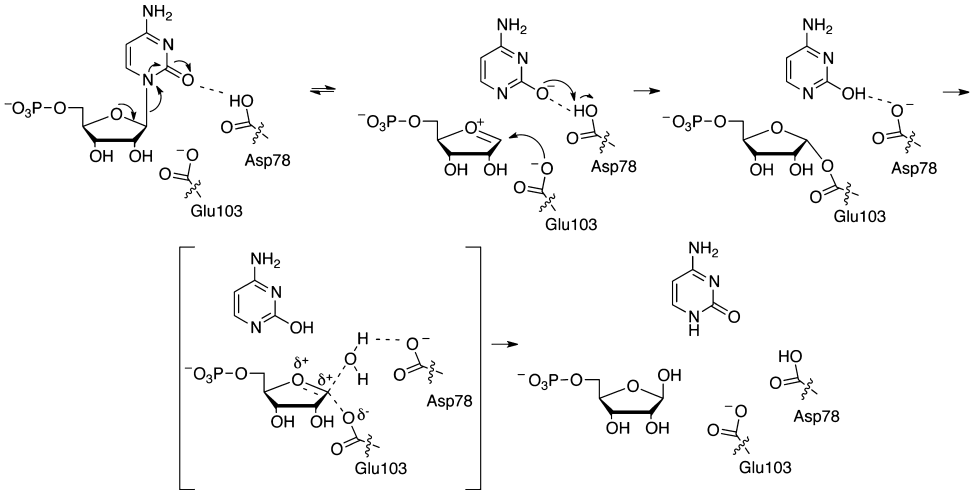

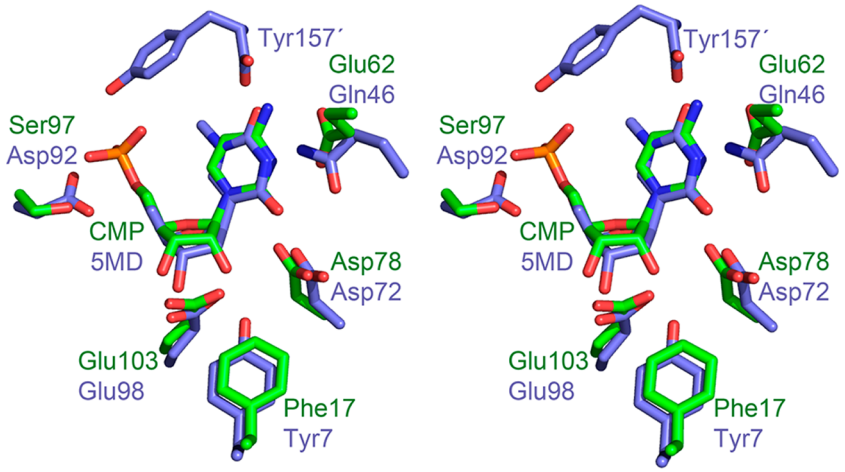

Figure 9. Active site comparison of MilB and NDT. A stereoview active site comparison between MilB with CMP bound (green) and NDT with 5-methyl-2′-deoxypseudouridine (5MD) (blue) reveals the conserved positioning of the catalytic glutamate and aspartate residues. Other key residues for substrate binding deviate between the two structures.

value of k_{cat}, which is significantly enhanced, while the K_M values are in a similar range. Additionally, MilB WT less efficiently hydrolyzes dCMP possibly because the 2′-group of dCMP cannot form any such hydrogen bonding interaction to orient it for catalysis. Thus, MilB WT catalytic residues are best positioned for hydrolysis of CMP with the aid of the 2′-hydroxyl group orienting CMP in the binding pocket. These observations would also apply to BcmB WT and F6Y, which show patterns in efficiency for hydrolysis of CMP and dCMP similar to those of MilB WT and F17Y.

■ ASSOCIATED CONTENT

Supporting Information

Table S1 and Figures S1 and S2. This material is available free of charge via the Internet at http://pubs.acs.org.

Accession Codes

The coordinates of MilB−SO_4, MilB−CMP, and BcmB−PO_4 complexes have been deposited in the Protein Data Bank as entries 4JEN, 4JEM, and 4JEL, respectively.

■ AUTHOR INFORMATION

Corresponding Author

*Department of Chemistry and Chemical Biology, Cornell University, Ithaca, NY 14853. E-mail: see3@cornell.edu. Telephone: (607) 255-7961. Fax: (607) 255-1227.

Funding

This work was supported by National Institutes of Health Grants GM73220 and T32GM008500 and by the Robert A. Welch Foundation (Grant A-0034 to T.P.B.). This work is based upon research conducted at the Advanced Photon Source on the Northeastern Collaborative Access Team beamlines, which are supported by Grant GM103403 from the National Institutes of Health. Use of the Advanced Photon Source is supported by the U.S. Department of Energy, Office of Basic Energy Sciences, under Contract DE-AC02-06CH11357.

Notes

The authors declare no competing financial interest.

■ ACKNOWLEDGMENTS

We thank Dr. Cynthia Kinsland for cloning MilB and BcmB and Leslie Kinsland for assistance in preparing the manuscript.

We thank the staff of the NE-CAT at the APS for assistance with data collection.

■ ABBREVIATIONS

NDT, nucleoside 2′-deoxyribosyltransferase; hmCMP, 5-hydroxymethylcytidine 5′-monophosphate; CMP, cytidine 5′-monophosphate; SeMet, selenomethionyl; AMP, adenosine 5′-monophosphate; IMP, inosine 5′-monophosphate; UMP, uridine 5′-monophosphate; dCMP, 2′-deoxycytidine 5′-monophosphate; GMP, guanosine 5′-monophosphate; SAD, single-wavelength anomalous diffraction; PTD, purine deoxyribosyltransferase; DMHA, *N*,*N*-dimethylhexylamine; 5MD, 5-methyl-2′-deoxypseudouridine; rmsd, root-mean-square deviation.

■ REFERENCES

(1) Li, L., Xu, Z., Xu, X., Wu, J., Zhang, Y., He, X., Zabriskie, T. M., and Deng, Z. (2008) The mildiomycin biosynthesis: Initial steps for sequential generation of 5-hydroxymethylcytidine 5′-monophosphate and 5-hydroxymethylcytosine in *Streptoverticillium rimofaciens* ZJU5119. *ChemBioChem 9*, 1286−1294.

(2) Feduchi, E., Cosin, M., and Carrasco, L. (1985) Mildiomycin: A nucleoside antibiotic that inhibits protein synthesis. *J. Antibiot. 38*, 415−419.

(3) Harada, S., and Kishi, T. (1978) Isolation and characterization of mildiomycin, a new nucleoside antibiotic. *J. Antibiot. 31*, 519−524.

(4) Macnutt, W. S. (1952) The enzymically catalysed transfer of the deoxyribosyl group from one purine or pyrimidine to another. *Biochem. J. 50*, 384−397.

(5) Chawdhri, R. F., Hutchinson, D. W., and Richards, A. O. (1991) Nucleoside Deoxyribosyltransferase and Inosine Phosphorylase-Activity in Lactic-Acid Bacteria. *Arch. Microbiol. 155*, 409−411.

(6) Armstrong, S. R., Cook, W. J., Short, S. A., and Ealick, S. E. (1996) Crystal structures of nucleoside 2-deoxyribosyltransferase in native and ligand-bound forms reveal architecture of the active site. *Structure 4*, 97−107.

(7) Ghiorghi, Y. K., Zeller, K. I., Dang, C. V., and Kaminski, P. A. (2007) The c-Myc target gene *Rcl* (C6orf108) encodes a novel enzyme, deoxynucleoside 5′-monophosphate *N*-glycosidase. *J. Biol. Chem. 282*, 8150−8156.

(8) Grochowski, L. L., and Zabriskie, T. M. (2006) Characterization of BlsM, a nucleotide hydrolase involved in cytosine production for the biosynthesis of blasticidin S. *ChemBioChem 7*, 957−964.

(9) Dupouy, C., Zhang, C., Padilla, A., Pochet, S., and Kaminski, P. A. (2010) Probing the active site of the deoxynucleotide *N*-hydrolase Rcl encoded by the rat gene c6orf108. *J. Biol. Chem. 285*, 41806−41814.

(10) Doddapaneni, K., Mahler, B., Pavlovicz, R., Haushalter, A., Yuan, C., and Wu, Z. (2009) Solution structure of RCL, a novel 2′-deoxyribonucleoside 5′-monophosphate *N*-glycosidase. *J. Mol. Biol. 394*, 423−434.

(11) Yang, Y., Padilla, A., Zhang, C., Labesse, G., and Kaminski, P. A. (2009) Structural characterization of the mammalian deoxynucleotide *N*-hydrolase Rcl and its stabilizing interactions with two inhibitors. *J. Mol. Biol. 394*, 435−447.

(12) Padilla, A., Amiable, C., Pochet, S., Kaminski, P. A., and Labesse, G. (2013) X-ray structure of the oncoprotein Rcl bound to three nucleotide analogs. *Acta Crystallogr. D69*, 247−255.

(13) Lewis, B. C., Shim, H., Li, Q., Wu, C. S., Lee, L. A., Maity, A., and Dang, C. V. (1997) Identification of putative c-Myc-responsive genes: Characterization of rcl, a novel growth-related gene. *Mol. Cell. Biol. 17*, 4967−4978.

(14) Shin, S., Bosc, D. G., Ingle, J. N., Spelsberg, T. C., and Janknecht, R. (2008) Rcl is a novel ETV1/ER81 target gene upregulated in breast tumors. *J. Cell. Biochem. 105*, 866−874.

(15) Sambrook, J., Fritsch, E. F., and Maniatis, T. (1989) *Molecular Cloning: A Laboratory Manual*, Vol. 3, Cold Spring Harbor Laboratory Press, Plainview, NY.

(16) Otwinowski, Z., and Minor, W. (1997) Processing of X-ray Diffraction Data Collected in Oscillation Mode. In *Methods in Enzymology* (Carter, C. W. J., and Sweet, R. M., Eds.) pp 307−326, Academic Press, New York.

(17) Matthews, B. W. (1968) Solvent content of protein crystals. *J. Mol. Biol. 33*, 491−497.

(18) Zwart, P. H., Afonine, P. V., Grosse-Kunstleve, R. W., Hung, L. W., Ioerger, T. R., McCoy, A. J., McKee, E., Moriarty, N. W., Read, R. J., Sacchettini, J. C., Sauter, N. K., Storoni, L. C., Terwilliger, T. C., and Adams, P. D. (2008) Automated structure solution with the PHENIX suite. *Methods Mol. Biol. 426*, 419−435.

(19) Adams, P. D., Afonine, P. V., Bunkoczi, G., Chen, V. B., Davis, I. W., Echols, N., Headd, J. J., Hung, L. W., Kapral, G. J., Grosse-Kunstleve, R. W., McCoy, A. J., Moriarty, N. W., Oeffner, R., Read, R. J., Richardson, D. C., Richardson, J. S., Terwilliger, T. C., and Zwart, P. H. (2010) PHENIX: A comprehensive Python-based system for macromolecular structure solution. *Acta Crystallogr. D66*, 213−221.

(20) Emsley, P., Lohkamp, B., Scott, W. G., and Cowtan, K. (2010) Features and development of Coot. *Acta Crystallogr. D66*, 486−501.

(21) Chen, V. B., Arendall, W. B., III, Headd, J. J., Keedy, D. A., Immormino, R. M., Kapral, G. J., Murray, L. W., Richardson, J. S., and Richardson, D. C. (2010) MolProbity: All-atom structure validation for macromolecular crystallography. *Acta Crystallogr. D66*, 12−21.

(22) Winn, M. D., Ballard, C. C., Cowtan, K. D., Dodson, E. J., Emsley, P., Evans, P. R., Keegan, R. M., Krissinel, E. B., Leslie, A. G., McCoy, A., McNicholas, S. J., Murshudov, G. N., Pannu, N. S., Potterton, E. A., Powell, H. R., Read, R. J., Vagin, A., and Wilson, K. S. (2011) Overview of the CCP4 suite and current developments. *Acta Crystallogr. D67*, 235−242.

(23) Vagin, A., and Teplyakov, A. (2000) An approach to multi-copy search in molecular replacement. *Acta Crystallogr. D56*, 1622−1624.

(24) Murshudov, G. N., Skubak, P., Lebedev, A. A., Pannu, N. S., Steiner, R. A., Nicholls, R. A., Winn, M. D., Long, F., and Vagin, A. A. (2011) REFMAC5 for the refinement of macromolecular crystal structures. *Acta Crystallogr. D67*, 355−367.

(25) Li, L., Xu, Z., Xu, X., Wu, J., Zhang, Y., He, X., Zabriskie, T. M., and Deng, Z. (2008) The mildiomycin biosynthesis: Initial steps for sequential generation of 5-hydroxymethylcytidine 5′-monophosphate and 5-hydroxymethylcytosine in *Streptoverticillium rimofaciens* ZJU5119. *ChemBioChem 9*, 1286−1294.

(26) DeLano, W. L. (2002) *The PyMOL Molecular Graphics System*, DeLano Scientific, San Carlos, CA.

(27) Holm, L., and Rosenstrom, P. (2010) Dali server: Conservation mapping in 3D. *Nucleic Acids Res. 38* (Suppl.), W545−W549.

(28) Anand, R., Kaminski, P. A., and Ealick, S. E. (2004) Structures of purine 2′-deoxyribosyltransferase, substrate complexes, and the ribosylated enzyme intermediate at 2.0 Å resolution. *Biochemistry 43*, 2384−2393.

(29) Bosch, J., Robien, M. A., Mehlin, C., Boni, E., Riechers, A., Buckner, F. S., Van Voorhis, W. C., Myler, P. J., Worthey, E. A., DeTitta, G., Luft, J. R., Lauricella, A., Gulde, S., Anderson, L. A., Kalyuzhniy, O., Neely, H. M., Ross, J., Earnest, T. N., Soltis, M., Schoenfeld, L., Zucker, F., Merritt, E. A., Fan, E., Verlinde, C. L., and Hol, W. G. (2006) Using fragment cocktail crystallography to assist inhibitor design of *Trypanosoma brucei* nucleoside 2-deoxyribosyltransferase. *J. Med. Chem. 49*, 5939−5946.

(30) Kaminski, P. A. (2002) Functional cloning, heterologous expression, and purification of two different *N*-deoxyribosyltransferases from *Lactobacillus helveticus*. *J. Biol. Chem. 277*, 14400−14407.

(31) Porter, D. J., Merrill, B. M., and Short, S. A. (1995) Identification of the active site nucleophile in nucleoside 2-deoxyribosyltransferase as glutamic acid 98. *J. Biol. Chem. 270*, 15551−15556.

(32) Tull, D., and Withers, S. G. (1994) Mechanisms of cellulases and xylanases: A detailed kinetic study of the exo-β-1,4-glycanase from *Cellulomonas fimi*. *Biochemistry 33*, 6363−6370.